RSC Advances

ROYAL SOCIETY OF CHEMISTRY

www.rsc.org/advances

Cite this: DOI: 10.1039/c0xx00000x

www.rsc.org/xxxxxx

PAPER

Heterogeneous nucleation capability of conical microstructures for water droplet

Wei Xu, Zhong Lan, Benli Peng, Rongfu Wen, and Xuehu Ma*

Received (in XXX, XXX) Xth XXXXXXXXX 20XX, Accepted Xth XXXXXXXXX 20XX
DOI: 10.1039/b000000x

The presence of micro structures on substrate has great effect on the heterogeneous nucleation of water droplet. A circular conical apex and a cavity are adopted as the physical model to represent the typical defects which widely exist on substrates, and the classic nucleation theory is used to quantitatively analyze the nucleation capability of different micro structures at different condensation conditions. The results indicate that the conical cavities with narrower cone angles can reduce the nucleation free energy barrier as compared with apexes and planar substrate, yielding a relatively higher nucleation capability. With the vapor pressure and supersaturation increasing, the nucleation rate increases rapidly, and a part of cavities that are originally not preferred for nucleation gradually translate into active nucleation sites. Consequently, the activated nucleation sites are finite for practical substrate under certain nucleation condition, and the nucleation sites number density can be affected by the condensation condition and the distribution of micro cavities on substrate. The analysis also indicated that it is possible to realize the spatial control of nucleation sites by the construction of micro cavities, and the nucleation sites number densities can be intensified by increasing the amount of micro cavities on the substrate.

1. Introduction

It can be observed that, when dew drops form, although they may be positioned randomly on flat leaves, they often tend to accumulate in the direction of leaf tip as time continues. The mechanism of this behavior has been reported by Shanahan [1] in terms of surface free energy minimization. Another question naturally arises is: why exactly the initial dew drop doses not preferably form at the leaf tip in the first place?

The formation of initial dew drop is a typical heterogeneous nucleation process of liquid droplet from bulk vapor phase, which is a typical process that exists in nature and industrial applications, such as the formation of rain drops and hailstones, crystal formation,[2-5] chemical vapor deposition,[6-8] and nucleation of initial droplets in dropwise condensation. As far as the nucleation process is concerned, the thermodynamic model was usually adopted and referred as the Classic Nucleation Theory (CNT).[9, 10] After then, the CNT model has been modified to obtain more accurate results,[11-14] and the effect of planar substrate and the heterogeneous nucleation model were considered.[15-24] Experimental results revealed that the nucleation process can be affected by artificially distributed hydrophilic area to realize the so called "spatial control" of nucleation sites.[25] On the other hand, the relationship between substrate structure and nucleation process,[26-33] and the effect of micro particles on the nucleation rate were also widely investigated.[34, 35] The results suggest that the initial droplets tend to appear on the substrate defects and deposited heterogeneous particles. [26, 27, 33] And the nucleation sites number density increases with the surface roughness. [28, 36] These results all indicated that the substrate properties, such as the wettability of substrate material, and the distribution of micro structures, have great effect on the nucleation of initial nucleus. However, most of the works concentrated on the physico-chemical properties that is obtained from statistics, such as the apparent contact angle and surface roughness. And the underlying mechanism on how the substrate structures affect nucleation process is still not very clear. Hence, a better understanding for the behavior of initial dew drop formation on different structures is very significant to explain the natural phenomenon and predict the effect of substrate structures on nucleation processes.

In this paper, the behavior of heterogeneous nucleation of water droplet on conical microstructures will be explored. A circular conical apex and a cavity are adopted as the physical model to represent the typical defects widely existing on the substrates, and the CNT model is adopted to quantitatively analyze the nucleation capability of the micro structures under different condensation conditions.

2. Physical model

A circular conical apex and a cavity are shown in Fig. 1 to represent the defects which exist in actual substrates, and a planar substrate is also considered for comparison. The structures are characterized by the intrinsic wetting angle α of substrate material and the cone angle β. As the initial nucleus is relatively small, the gravitational force can be neglected as compared with the surface tension effect. According to the classic capillary approximation[16] and the molecular dynamics simulation results,[37] the nucleus will deposited on three different substrate structures in the form of spherical cap as shown in Fig. 1, with the local contact angle equal to the intrinsic wetting angle of the substrate material. It has to be pointed out that, for structures fulfill the condition of $\alpha+\beta/2<90°$, the meniscus within micro cavities will be in a

concave manner instead of that described in Fig. 1c. The additional pressure provided by the concave meniscus is favorable for the stability of embryos of any sizes and hence is favorable for the formation of nucleus. Based on this fact, the structures fulfill $\alpha+\beta/2<90°$ condition will not be considered in this paper. The sizes of microstructures are comparable to that of initial nucleus, which is in nanoscale under typical nucleation condition of water droplet.

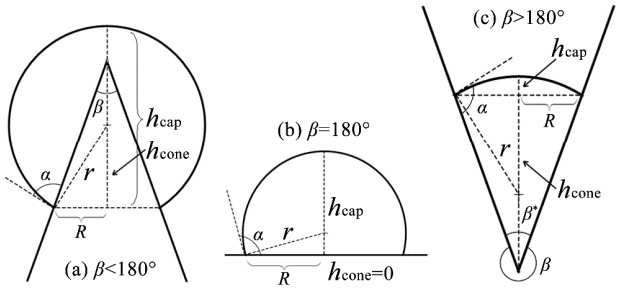

Fig. 1 Schematic representation of an axisymmetric nucleus on three micro structures. (a) circular conical apex, (b) planar substrate, (c) circular conical cavity

In the following thermodynamic model section, it can be found that the nucleation process is greatly affected by the volume and liquid-vapor and liquid-solid interfacial areas of the initial nucleus. For a nucleus deposited on an apex as described by Fig. 1a, the related parameters can be calculated from geometry:

$$R = r^* \times \cos(\alpha - \beta/2) \tag{1}$$

$$h_{cap} = r^* \times [1 + \sin(\alpha - \beta/2)] \tag{2}$$

$$h_{cone} = R \times \cot(\beta/2) \tag{3}$$

where r^* is the critical curvature radius of initial nucleus, R is the bottom radius of the cone, h_{cap} and h_{cone} are the heights of the spherical cap and the cone, respectively.

The volume of nucleus V_{drop}, the liquid-vapor and liquid-solid interfacial areas of S_{lv} and S_{ls} can be obtained as follows:

$$V_{drop} = \frac{\pi r^{*3}}{3}\left[\begin{array}{l} 2+3\sin\left(\alpha-\frac{\beta}{2}\right)-\sin^3\left(\alpha-\frac{\beta}{2}\right) \\ -\cos^3\left(\alpha-\frac{\beta}{2}\right)\cot\frac{\beta}{2} \end{array}\right] \tag{4}$$

$$S_{lv} = 2\pi r^{*2}[1+\sin(\alpha-\beta/2)] \tag{5}$$

$$S_{ls} = \pi r^{*2}\cos^2(\alpha-\beta/2)/\sin(\beta/2) \tag{6}$$

In the case of planar substrate, β can be simply set as 180°. For a cavity structure, the cone angle β^* can be converted into β by a formula $\beta=360-\beta^*$, and the formulas above are also applicable. Consequently, Eq. (1) ~ (6) can be used to calculate the parameters related for all three physical structures.

3. Thermodynamic model

Generally, the nucleation capability at certain condition can be evaluated either by the nucleation free energy barrier $\Delta G(r^*)$ or the nucleation rate J. Here, $\Delta G(r^*)$ is defined as the Gibbs free energy barrier that has to be overcome to form a nucleus of critical size r^*; J is defined as the number of initial nuclei formed within unit time period and unit volume or area for homogeneous or heterogeneous nucleation processes. Based on classic nucleation theory, the nucleation rate J can be expressed as follows:[19, 25]

$$J = J_0 \exp\left(-\frac{\Delta G(r^*)}{k_B T}\right) \tag{7}$$

where J_0 is a kinetic pre-factor that is directly connected with vapor conditions and nucleus configurations (spherical shape for homogeneous nucleation, and spherical cap for heterogeneous nucleation on planar substrate).[19, 38] k_B is the Boltzmann constant, T is the temperature.

For the CNT model, the capillary approximation[16, 19, 21] and Young's equation, the nucleation free energy barrier of critical nucleus can be expressed as:

$$\Delta G(r^*) = -\frac{\rho V_{drop}}{M} N_A k_B T \ln S + \sigma_{lv}(S_{lv} - S_{ls}\cos\alpha) \tag{8}$$

where ρ, σ_{lv} and M are the density, surface tension and molecular mass of condensate liquid, respectively. According to capillary assumption[16, 19, 21], ρ and σ_{lv} are obtained from the physico-chemical properties of bulk liquid. N_A is the Avogadro's number. S is the supersaturation defined as the ratio between vapor pressure P_v and the equilibrium pressure at nucleation temperature.

The critical radius of nucleus can be obtained as:[25]

$$r^* = \frac{2\sigma_{lv}}{n_l k_B T \ln S} \tag{9}$$

where n_l is the number of molecules per unit volume of condensate liquid.

Substitute Eq. (9) into Eq. (4) ~ (6) to calculate V_{drop}, S_{lv} and S_{ls}, and then substitute them into Eq. (8), a general formula of $\Delta G(r^*)$ can be obtained as follows with respect to the micro structure configurations:

$$\Delta G(r^*) = \frac{4\pi\sigma_{lv} r^{*2}}{3} F(\alpha, \beta) \tag{10}$$

with $F(\alpha, \beta)$ the form factor that is connected with substrate structure parameters , written in the following expressions:

$$F(\alpha,\beta) = \frac{1}{4}\left[\begin{array}{l} 2+3\sin\left(\alpha-\frac{\beta}{2}\right)-\sin^3\left(\alpha-\frac{\beta}{2}\right) \\ -\cos^3\left(\alpha-\frac{\beta}{2}\right)\cot\frac{\beta}{2} \end{array}\right] \tag{11}$$

For nucleation processes of liquid droplets from bulk vapor phase, the nucleation rate J can be deduced form the following simplified general formula:[21]

$$J = \left\{\int_0^\infty \left[N(n)\cdot j_e(n)\cdot A(n)\right]^{-1} \mathrm{d}n\right\}^{-1} \tag{12}$$

where $N(n)$ is the number density of embryos containing n molecules per unit area for heterogeneous nucleation, $j_e(n)$ is the attachment rate of vapor molecules onto an embryo of size n, $A(n)$ is the vapor-liquid interfacial area of an embryo. The term of embryo is adopted to denote a molecular cluster that has not reach up to the critical size, in order to differentiate from nucleus.

The integral formula in Eq. (12) means that the nuclei are developed from embryos with various sizes. The number distribution of these embryos $N(n)$ can be obtained from the classic cluster size distribution model:[11, 21, 24]

$$N(n) = \rho_{\mathrm{N,\,v}}^{2/3} \exp\left(-\frac{\Delta G(r)}{k_{\mathrm{B}}T}\right) \tag{13}$$

where $\rho_{\mathrm{N,\,v}}$ is the number of vapor molecules per unit volume of the bulk vapor. The pre-factor of the above formula is either $\rho_{\mathrm{N,\,v}}$ or $(\rho_{\mathrm{N,\,v}})^{2/3}$ for homogeneous or heterogeneous nucleation.[21] In the present study, the nucleation occurs on substrate, and the pre-factor of $(\rho_{\mathrm{N,\,v}})^{2/3}$ is used. The analysis is conducted under steady state conditions, and there is no depletion effects on the finite number of microstructures. $\Delta G(r)$ is the free energy change for the formation of embryo of radius r. The difference between $\Delta G(r)$ and $\Delta G(r^*)$ is whether the critical radius is achieved.

The radius of the embryo r is related to the number of molecules n in the embryo by:

$$\frac{4\pi r^3}{3} F(\alpha,\,\beta) = n m v_{\mathrm{l}} \tag{14}$$

where m is the mass of one molecule, v_{l} is the specific volume of the condensate, which is also adopted from bulk liquid.[16, 19, 21]

$\Delta G(r)$ can be obtained by expanding the right hand side term of Eq. (10) in a Taylor power series in terms of r-r^* about the equilibrium radius r^*:[21]

$$\Delta G(r) = \frac{4\pi\sigma_{\mathrm{lv}} r^{*2}}{3} F(\alpha,\,\beta) - 4\pi\sigma_{\mathrm{lv}} F(\alpha,\,\beta)\cdot\left(r - r^*\right)^2 + \cdots \tag{15}$$

$j_e(n)$ can be deduced from the kinetic theory of gases:

$$j_{\mathrm{e}}(n) = \frac{P_{\mathrm{v}}}{\sqrt{2\pi m k_{\mathrm{B}} T}} \tag{16}$$

With the consideration of micro structure configurations, the interfacial area of $A(n)$ can be expressed as:

$$A(n) = 2\pi r^2\left[1 + \sin\left(\alpha - \beta/2\right)\right] \tag{17}$$

Substitute Eq. (13), (16) and (17) into Eq. (12), the nucleation rate J writes:

$$J = \left\{\int_0^{\infty}\left[\frac{2\pi r^2 \rho_{\mathrm{N,v}}^{2/3} P_{\mathrm{v}}}{\sqrt{2\pi m k_B T}} \times \exp\left(-\frac{\Delta G(r)}{k_{\mathrm{B}}T}\right) \times\left[1+\sin\left(\alpha-\beta/2\right)\right]\right]^{-1} \mathrm{d}n\right\}^{-1} \tag{18}$$

Meanwhile, the relationship between cluster size n and r can be described by Eq. (14). Substitute Eq. (14) into the above formula, J can be organized as:

$$J = \frac{\rho_{\mathrm{N,v}}^{2/3} P_{\mathrm{v}} m v_{\mathrm{l}}\left[1+\sin\left(\alpha-\beta/2\right)\right]}{2F(\alpha,\beta)\sqrt{2\pi m k_B T}}\left\{\int_0^{\infty}\exp\left(\frac{\Delta G(r)}{k_{\mathrm{B}}T}\right)\mathrm{d}r\right\}^{-1} \tag{19}$$

Substitute Eq. (15) into the integration term of the above formula, we can get:

$$\int_0^{\infty}\exp\left(\frac{\Delta G(r)}{k_{\mathrm{B}}T}\right)\mathrm{d}r = \left[\begin{array}{l}\exp\left(\dfrac{4\pi r^{*2}\sigma_{\mathrm{lv}}F(\alpha,\beta)}{3k_{\mathrm{B}}T}\right) \\ \times\displaystyle\int_0^{\infty}\exp\left(-\frac{4\pi\sigma_{\mathrm{lv}}F(\alpha,\beta)}{k_{\mathrm{B}}T}\left(r-r^*\right)^2\right)\mathrm{d}r\end{array}\right] \tag{20}$$

Set intermediate variable B as:

$$B = \left[\frac{4\pi\sigma_{\mathrm{lv}}F(\alpha,\beta)}{k_{\mathrm{B}}T}\right]^{1/2}\left(r - r^*\right) \tag{21}$$

Eq. (20) then can be simplified as follows:

$$\begin{aligned}\int_0^{\infty}\exp\left(\frac{\Delta G(r)}{k_{\mathrm{B}}T}\right)\mathrm{d}r &= \left[\begin{array}{l}\exp\left(\dfrac{4\pi r^{*2}\sigma_{\mathrm{lv}}F(\alpha,\beta)}{3k_{\mathrm{B}}T}\right) \\ \times\left(\dfrac{k_{\mathrm{B}}T}{4\pi\sigma_{\mathrm{lv}}F(\alpha,\beta)}\right)^{1/2}\times\displaystyle\int_{-\infty}^{\infty}\exp\left(-B^2\right)\mathrm{d}B\end{array}\right] \\ &= \left(\frac{k_{\mathrm{B}}T}{4\sigma_{\mathrm{lv}}F(\alpha,\beta)}\right)^{1/2}\exp\left(\frac{4\pi r^{*2}\sigma_{\mathrm{lv}}F(\alpha,\beta)}{3k_{\mathrm{B}}T}\right)\end{aligned} \tag{22}$$

Finally, substitute Eq. (22) into Eq. (19), a general form of J can be obtained as:

$$J = \left(\frac{P_{\mathrm{v}}}{k_{\mathrm{B}}T}\right)^{5/3} v_{\mathrm{l}}\left(\frac{2\sigma_{\mathrm{lv}}m}{\pi}\right)^{1/2}\frac{1+\sin\left(\alpha-\beta/2\right)}{2\sqrt{F(\alpha,\,\beta)}}\exp\left(-\frac{\Delta G(r^*)}{k_{\mathrm{B}}T}\right) \tag{23}$$

If β is taken to be 180°, Eq. (23) becomes identical to the expression for heterogeneous nucleation on planar substrate.

Meanwhile, the kinetic pre-factor J_0 in Eq. (7) also can be obtained as:

$$J_0 = \left(\frac{P_{\mathrm{v}}}{k_{\mathrm{B}}T}\right)^{5/3} v_{\mathrm{l}}\left(\frac{2\sigma_{\mathrm{lv}}m}{\pi}\right)^{1/2}\frac{1+\sin\left(\alpha-\beta/2\right)}{2\sqrt{F(\alpha,\,\beta)}} \tag{24}$$

As indicated by Eq. (10) and Eq. (23), the nucleation rate J is a function of nucleation conditions (P_{v} and S) and substrate structure parameters (α, β).

4. Results and discussion

4.1 Effect of β on the nucleation rate

According to Eq. (23), the nucleation rate of heterogeneous nucleation process is determined by J_0 and $\Delta G(r^*)$. The calculated results of J_0 and $\Delta G(r^*)$ under various structure parameters are shown in Fig. 2. As β increases, the substrate structures translate from apexes to cavities, with J_0 and $\Delta G(r^*)$ decreasing rapidly in the same manner. As indicated by the schematic diagram of the physical model, a relatively larger liquid-vapor interfacial area is expected for an initial nucleus deposited on the top of an apex, providing a relatively higher probability for vapor molecular

attachment. As a result, J_0 is larger for an apex than that of planar substrate or cavities. For instance, the calculated results of J_0 for an apex with β=60° is 1.37 times than that of planar substrate (β=180°) and 3.73 times than that of a cavity with β=300° (β^*=60°). On the other hand, as β increases, the volume and interfacial area of initial nucleus decrease accordingly due to the space-confining effect of cavities. Considering that the main part of the nucleation free energy barrier is caused by the formation of new interfaces, the decrease of interfacial area is thus favorable for the decrease of $\Delta G(r^*)$. For instance, $\Delta G(r^*)$ for an apex with β=60° is 1.87 times that of planar substrate and 13.93 times than that of a cavity with β=300°.

It is necessary to point out that, as the nucleation rate is an exponential function of $\Delta G(r^*)$, the nucleation free energy barrier is thus decisive to the heterogeneous nucleation processes. According to Eq. (23), the nucleation rate for a cavity with β^*=60° is 9.0×10^{32} times than that of planar substrate and 1.6×10^{66} times than that of an apex with β=60° under considered nucleation condition. As the micro structures translate from apexes to cavities, comparably lower nucleation free energy barriers are required to form initial nucleus due to the space-confining effect of cavities, and the nucleation rates are thus increased. Based on the discussions above, the order of the nucleation capability of three structure configurations are cavities, planar substrate and apexes. The presences of cavities with narrower cone angles are favorable for nucleation processes.

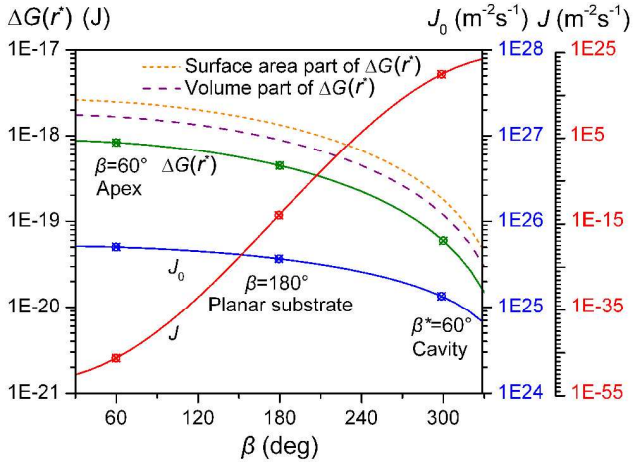

Fig. 2 $\Delta G(r^*)$, J_0 and J under various structure parameters. (P_v=100 kPa, S=1.5, α=90°)

The nucleation rate J calculated from Eq. (23) is shown in Fig. 3, under the nucleation condition of P_v=100 kPa, S=1.5. Apexes are not considered as they are not preferred for nucleation comparing with planar substrate and cavities. The structure parameter β is translated into β^* using the relation of β^*=360-β, and a smaller β^* denotes a narrower cavity. The intrinsic wetting angle α is restricted within 60~110° with the consideration of most practical substrate materials.[21] As expected, the nucleation rate decreases with α sharply, indicating that the nucleation rate on hydrophilic surface was higher than a hydrophobic one for any substrate structures. Meanwhile, the nucleation rates for narrower cavities are obviously greater than the planar substrate for the same α, indicating relatively higher nucleation capabilities for micro cavities. It has been reported by Varanasi[25] that the nucleation rate on a hydrophilic surface with α~25° is about 10^{129} times higher than that on a hydrophobic surface with α~110°, and the nucleation sites can be artificially controlled by a hydrophilic-hydrophobic hybrid surface. According to the model analysis above, the so called spatial control of nucleation sites also can be realized by the appropriate substrate structure constructions, except for the regulation of surface wettability.

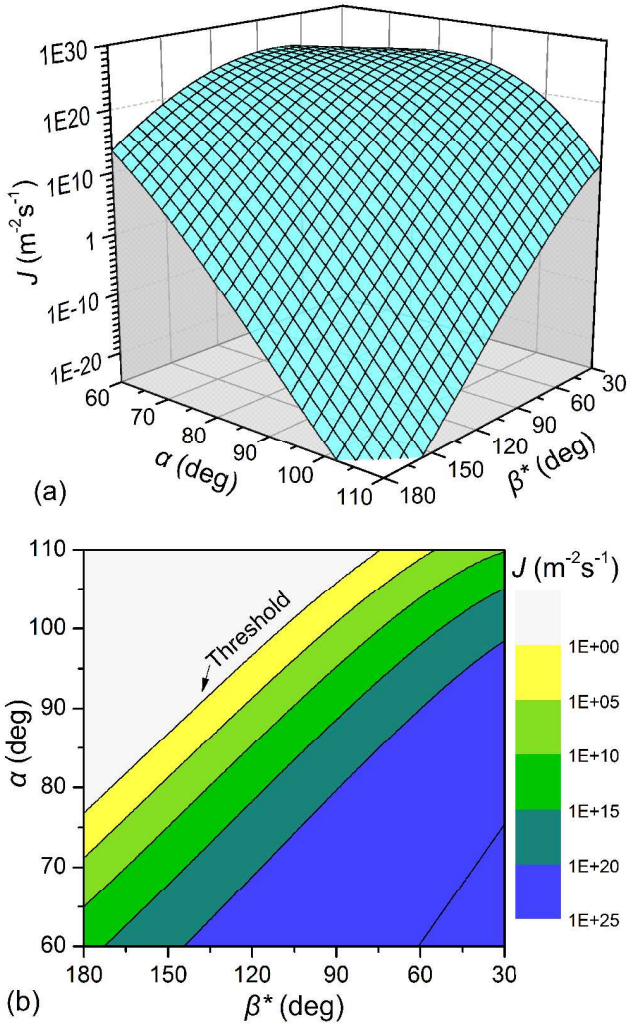

Fig. 3 Nucleation rate as a function of wetting angle α and structure parameter β^*. (P_v=100 kPa, S=1.5)

It also can be found that, the effect of structure parameter is so great that the nucleation rates under certain conditions are extremely low and almost no nucleus can be formed under these circumstances. This behavior actually provides a threshold of α and β for the heterogeneous nucleation processes. In the contour map of Fig. 3, a threshold of 1 $m^{-2}s^{-1}$ is chosen following Carey's analysis.[21] As a result, only those micro cavities that fulfill the threshold can be activated to form initial nuclei (see the lower-right part of the contour map with color fill).

For water vapor condensation, the kinetic pre-factor J_0 is usually in the range of 10^{23}~10^{26} $m^{-2}s^{-1}$, which means that the exponential part of Eq. (23) has to be greater than 10^{-26}~10^{-23} to fulfill the threshold. The threshold proposed here actually provides an upper limit for the nucleation free energy barrier. To

ensure effective nucleation, $\Delta G(r^*)$ has to be lower enough, and the upper limit of $\Delta G(r^*)$ can be calculated from Eq. (23) at different condensation conditions. In principle, a relatively lower wetting angle and narrower cavity are favorable for nucleation processes. This also explains why the randomly distributed cavities, grooves, scratches (smaller β^*) and heterogeneous particles (smaller α) can act as nucleation sites.[26, 27, 39]

One of the important characters obtained from the above analysis is that the number of active nucleation sites will be finite on a practical condensation substrate with randomly distributed micro cavities. The number of nucleation sites per unit surface area is usually defined as the nucleation sites number density (N_s), an important parameter in dropwise condensation heat transfer theory.[40] Considering that the actual condensation substrate is composed of randomly distributed micro cavities, grooves and apexes of different structure parameters, the nucleation capabilities of different areas are inherently different depending on whether the above threshold are well fulfilled. During the initial condensation stage, the micro cavities with higher nucleation capabilities will be rapidly occupied by initial nuclei. As condensation continues, more cavities that fulfill the threshold will be gradually activated, and the number of initial nuclei increases accordingly until all of the possible nucleation sites are occupied, yielding a maximum value of nuclei numbers. After that, the subsequent condensation process will be realized by the growth of pre-existed nuclei from critical size to micro droplets, while no nucleus could form on the blank surface between adjacent droplets. The blank area is inherently not preferred for nucleation basically due to the failure to fulfill the threshold.

4.2 Nucleation capability of micro cavities at various condensation conditions

As indicated by Eq. (9) and Eq. (23), the nucleation rate is also a function of vapor pressure and supersaturation. The calculated results of nucleation rate at various condensation conditions are presented in Fig. 4 and Fig. 5, with S varying from 1.2 to 1.6 under the vapor pressure of 100 kPa, and P_v varying from 10 kPa to 100 kPa under the supersaturation of 1.5, respectively. As described earlier, an arbitrary threshold of J=1 $m^{-2}s^{-1}$ is chosen to determine whether the micro cavity can be activated as an nucleation site, and the combination of α and β that fulfill the threshold are shown in Fig. 4 and Fig. 5 by color fill.

As S increases from 1.2 to 1.6, the nucleation rate for the same structure increases accordingly. According to Eq. (9), the critical size of nucleus decreases sharply as S increases, yielding a comparably lower nucleation free energy barrier as indicated by Eq. (10). Consequently, the nucleation rate is greatly increased for the same micro cavity. Meanwhile, a part of micro cavities that is originally not preferred for nucleation under low supersaturations can translate into effective nucleation sites when S is increased to a certain degree.

On the other hand, the nucleation rate also increases with P_v under a constant supersaturation, as shown in Fig. 5. According to Eq. (9) and Eq. (10), as vapor pressure increases, the critical radius of nucleus decreases slightly, yielding a relatively lower nucleation free energy barrier that is preferred for nucleation. Meanwhile, as indicated by Eq. (24), the kinetic pre-factor J_0 also increases with P_v. As a result, J increases rapidly with P_v for the same S and α~β. Similar with the behavior observed in Fig. 4, a part of micro cavities that is originally not preferred for nucleation under low vapor pressures can translate into effective nucleation sites when P_v is increased to a certain degree, as shown in Fig. 5. As P_v and S increase, more micro cavities with wider cone angles can translate into active nucleation sites, suggesting that N_s may increase with P_v and S accordingly. The relationship between N_s and condensation condition has been noticed by different researchers,[41, 42] and the results also suggest that N_s increase with P_v and S.

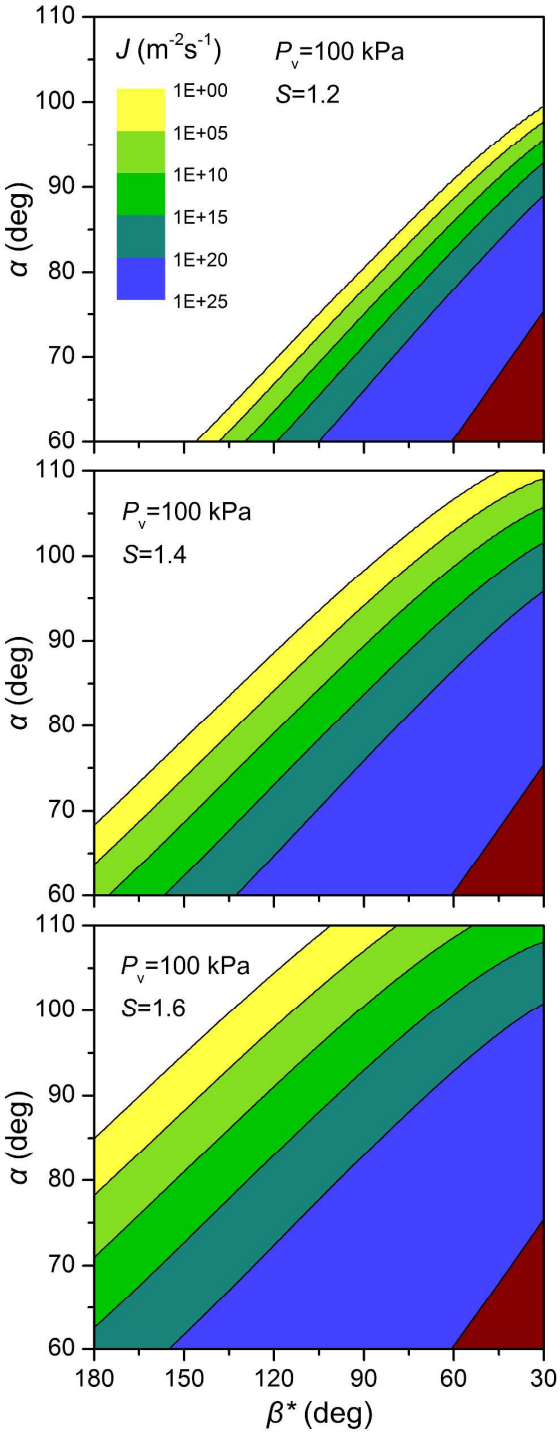

Fig. 4 Nucleation capability of micro cavities under various supersaturations.

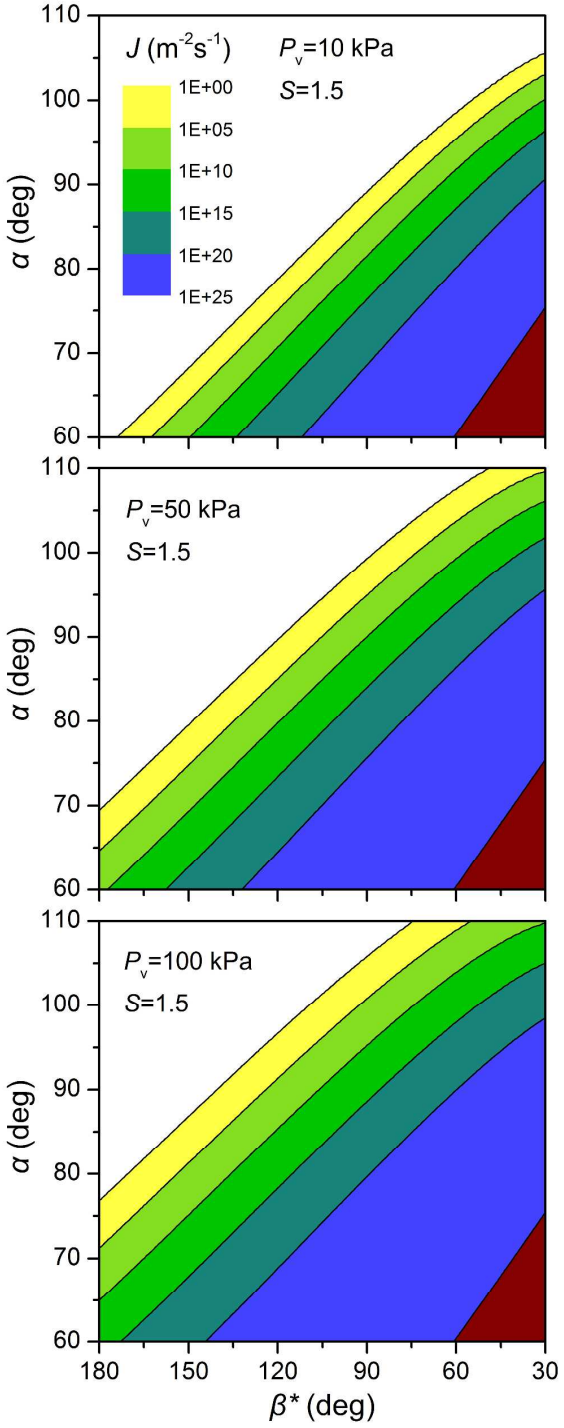

Fig. 5 Nucleation capability of micro cavities under various vapor pressures.

Conclusions

A circular conical apex and a cavity are proposed as physical models to represent the typical defects which widely exist on substrates, and the classic nucleation theory is adopted to quantitatively analyze the nucleation capability of different micro structures at different water vapor nucleation conditions.

The results indicate that the kinetic pre-factor and nucleation free energy barrier all decrease when the substrate structures translate from apexes to cavities, and the nucleation rate of narrower cavities are higher than planar substrate and apexes. The cavities that distributed on substrate can act as nucleation sites, and the activated nucleation sites are finite for practical substrates due to the different nucleation capabilities of different surface areas. The spatial control of nucleation sites and the intensification of nucleation sites number density can be realized by substrates with relatively lower wetting angle and the presence of narrower cavities.

The nucleation capability also can be affected by condensation conditions. As vapor pressure and supersaturation increase, the nucleation rate increases rapidly for the same structures, and a part of cavities that are originally not preferred for nucleation gradually translate into active nucleation sites, suggesting that the nucleation sites number density may increase with vapor pressure and supersaturation.

Acknowledgement

The authors greatly appreciate the financial support from the National Natural Science Foundation of China (No.51236002, No. 51476018).

Notes and references

Liaoning Provincial Key Laboratory of Clean Utilization of Chemical Resources, Institute of Chemical Engineering, Dalian University of Technology, Dalian, China, Fax/Tel: 86 411 84707892, E-mail: xuehuma@dlut.edu.cn

1 M. E. R. Shanahan, *Langmuir*, 2011, **27**, 14919-14922.
2 V. G. Karpov, Y. A. Kryukov, M. Mitra and I. V. Karpov, *J. Appl. Phys*., 2008, **104**, 054507.
3 A. T. Appapillai, C. Sachs and E. M. Sachs, *J. Appl. Phys*., 2011, **109**, 084916.
4 Z. Kožíšek and P. Demo, *J. Cryst. Growth*, 1998, **194**, 239-246.
5 S. Klein and D. M. Herlach, *J. Appl. Phys*., 2013, **114**, 183510.
6 S. A. Moshkalev and C. Verssimo, *J. Appl. Phys*., 2007, **102**, 044303.
7 Y. K. Chae and H. Komiyama, *J. Appl. Phys*., 2001, **90**, 3610-3613.
8 J. Robertson, *J. Appl. Phys*., 2003, **93**, 731-735.
9 M. Volmer and A. Weber, *Z. Phys. Chem*., 1926, **119**, 277-301.
10 J. C. Fisher, J. H. Hollomon and D. Turnbull, *J. Appl. Phys*., 1948, **19**, 775-784.
11 A. Dillmann and G. E. A. Meier, *J. Chem. Phys*., 1991, **94**, 3872-3884.
12 C. F. Delale and G. E. A. Meier, *J. Chem. Phys*., 1993, **98**, 9850-9858.
13 I. J. Ford, A. Laaksonen and M. Kulmala, *J. Chem. Phys*., 1993, **99**, 764-765.
14 V. I. Kalikmanov and M. E. H. Van Dongen, *J. Chem. Phys*., 1995, **103**, 4250-4255.
15 D. Turnbull, *J. Chem. Phys*., 1950, **18**, 198-203.
16 N. H. Fletcher, *J. Chem. Phys*., 1958, **29**, 572-576.
17 A. Laaksonen, I. J. Ford and M. Kulmala, *Phys. Rev. E*, 1994, **49**, 5517-5524.
18 V.Talanquer and D. W. Oxtoby, *Physica A*, 1995, **220**, 74-84.
19 D. Kashchiev, *Nucleation: Basic Theory with Applications*, Butterworth-Heinemann, Burlington, MA, 2000, ch. 3, pp. 32-33, ch. 9, pp. 124-125.
20 M. Qian, *Acta Mater*., 2007, **55**, 943-953.
21 V. P. Carey, *Liquid-vapor Phase-Change Phenomena*, Taylor and Francis, New York, USA, 2008.
22 C. M. L. V. Kroon and I. J. Ford, *Atmospheric Research*, 2011, **101**, 553-561.
23 A. S. Abyzov and J. W. P. Schmelzer, *J. Chem. Phys*., 2013, **138**, 164504.
24 W. Xu, Z. Lan, B. L. Peng, R. F. Wen and X. H. Ma, *RSC Adv.*, 2014, **4**, 31692-31699.

25 K. K. Varanasi, M. Hsu, N. Bhate, W. Yang and T. Deng, *Appl. Phys. Lett.*, 2009, **95**, 094101.
26 J. L. McCormick and J. W. Westwater, *Chem. Eng. Sci.*, 1965, **20**, 1021-1036.
27 T. Y. Song, Z. Lan, X. H. Ma and T. Bai, *Int. J. Therm. Sci.*, 2009, **48**, 2228-2236.
28 C. F. Mu, J. J. Pang, Q. Y. Lu and T. Q. Liu, *Chem. Eng. Sci.*, 2008, **63**, 874-880.
29 X. M. Chen, J. Wu, R. Y. Ma, M. Hua, N. Koratkar, S. H. Yao and Z. K. Wang, *Adv. Funct. Mater.*, 2011, **21**, 4617-4623.
30 E. Ruckenstein and G. O. Berim, *J. Colloid Interf. Sci.*, 2010, **351**, 277-282.
31 M. Qian and J. Ma, *J. Cryst. Growth*, 2012, **355**, 73-77.
32 K. Y. Li, S. Xu, W. X. Shi, M. He, H. L. Li, S. Z. Li, X. Zhou, J. J. Wang and Y. L. Song, *Langmuir*, 2012, **28**, 10749-10754.
33 C. W. Lo, C. C. Wang and M. C. Lu, *Adv. Funct. Mater.*, 2014, **24**, 1211-1217.
34 M. Lazaridis and Ø. Hov, *Atmospheric Research*, 2000, **55**, 103-113.
35 V. Y. Smorodin and P. K. Hopke, *Atmospheric Research*, 2006, **82**, 591-604.
36 I. O. Ucar and H. Y. Erbil, *Applied Surface Science*, 2012, **259**, 515-523.
37 A. Shahraz, A. Borhan and K. A. Fichthorn, *Langmuir*, 2013, **29**, 11632-11639.
38 J. W. P. Schmelzer, *Journal of Non-Crystalline Solids*, 2010, **356**, 2901-2907.
39 K. Rykaczewski, *Langmuir*, 2012, **28**, 7720-7729.
40 S. Kim and K. J. Kim, *J. Heat Transfer*, 2011, **133**, 081502.
41 C. Graham and P. Griffith, *Int. J. Heat Mass Transfer*, 1973, **16**, 337-346.
42 J. W. Rose, *Int. J. Heat Mass Transfer*, 1976, **19**, 1363-1370.